Kinetics of Isothermal Melt Crystallization in CaO-SiO_2-CaF_2-Based Mold Fluxes

MYUNG-DUK SEO, CHENG-BIN SHI, JI-YEON BAEK, JUNG-WOOK CHO, and SEON-HYO KIM

A kinetic study for isothermal melt crystallization of CaO-SiO_2-CaF_2-based mold fluxes with different basicity of 0.94 and 1.34 has been carried out systematically by DSC measurements. The kinetic parameters were determined by Johnson–Mehl–Avrami equation. The average Avrami exponent of cuspidine ($3CaO{\cdot}2SiO_2{\cdot}CaF_2$) crystallization for mold flux of lower basicity (0.94) is calculated to be 3.1, implying that the crystallization mode is instantaneous nucleation followed by 3-dimensional growth. For the mold flux of higher basicity (1.34), the average Avrami exponent of cuspidine equals to 3.4, strongly suggesting that the growth is still 3 dimensional but the nucleation should be continuous. It was found that the effective crystallization rate constant for both mold fluxes increases as the crystallization temperature decreases, showing that the crystallization rate could be governed by nucleation rate. The negative effective activation energy indicates an anti-Arrhenius behavior for crystallization of the mold fluxes studied. Therefore, it is concluded that the melt crystallization for the commercial mold fluxes will be determined by thermodynamics of nucleation which is relevant to degree of undercooling. The morphology of cuspidine crystals observed by SEM agreeds well with the isothermal crystallization kinetics results.

DOI: 10.1007/s11663-015-0358-2

I. INTRODUCTION

In continuous casting of steel, commercial mold fluxes have been mainly used to control the horizontal mold heat transfer and to lubricate the solidified steel shell from oscillating mold.[1] It is well known that the heat transfer and the lubrication are strongly dependent on the crystallization behaviors of mold fluxes such as extent and morphology of crystalline phase,[2–7] which are determined by nucleation and crystal growth. Therefore, it is highly required to understand crystallization kinetics of mold fluxes to improve the performance of continuous casting process. A few studies[8–10] have been conducted to investigate the crystallization kinetics that occurs on heating. However, it should be stressed that these studies[8–10] are limited in revealing the crystallization behavior of commercial mold fluxes which should be regarded as one of melt crystallization during cooling on the copper mold.

For the purpose of overcoming the limitation, investigations[11–18] on non-isothermal melt crystallization kinetics have been carried out. Choi[11] and Gan *et al.*[12] had adapted well-known Kissinger and Matusita equations and obtained positive value of activation energy for melt crystallization. However, it is unreasonable to apply those equations on non-isothermal melt crystallization because Kissinger and Matusita equations are initially derived from assumptions in that crystallization occurs on heating. Vyazovkin[19,20] clarified that invalid results will be derived by direct application of these equations to any non-isothermal melt crystallization. Recently, the present authors[21] critically proposed problems of these approaches and concluded that Kissinger and Matusita equation is not applicable in obtaining activation energy of non-isothermal melt crystallization. It was additionally found that Ozawa equation was not suitable to evaluate kinetic parameters of non-isothermal melt crystallization for the mold fluxes[13,14] as well as polymer system.[15–18] As a possible alternative to this problem, the differential iso-conversional method developed by Freidman[22] has been successfully employed to evaluate non-isothermal melt crystallization kinetics.[13,14,23–25] However, it should be interestingly noticeable that aforementioned Friedman method[22] has limitations in obtaining quantitative kinetic parameters such as Avrami constant n and crystallization rate k.

In order to quantitatively evaluate kinetic parameters for crystallization of mold fluxes, investigations[26–29] on isothermal melt crystallization kinetics have been conducted using the single or double hot thermocouple technique (SHTT/DHTT). Although there has been tremendous progress on kinetics of mold flux melt crystallization, these studies are limited in acquiring

MYUNG-DUK SEO and JI-YEON BAEK, Ph.D. Candidates, and SEON-HYO KIM, Professor are with the Department of Materials Science and Engineering, Pohang University of Science and Technology (POSTECH), Pohang 790-784, Republic of Korea. CHENG-BIN SHI, Assistant Professor, is with the State Key Laboratory of Advanced Metallurgy, University of Science and Technology Beijing (USTB), Beijing 100083, P.R. China. JUNG-WOOK CHO, Research Associate Professor, is with the Graduate Institute of Ferrous Technology, Pohang University of Science and Technology (POSTECH), Pohang 790-784, Republic of Korea. Contact e-mail: jungwook@postech.ac.kr

Manuscript submitted December 23, 2014.
Article published online April 30, 2015.

accurate crystalline fraction, which is a crucial parameter for knowing kinetic parameters such as Avrami exponent n, effective crystallization rate constant k, and crystallization activation energy, due to the fact that SHTT/DHTT only provides two-dimensional information on crystallization kinetics.

In this study, the isothermal melt crystallization kinetics of $CaO\text{-}SiO_2\text{-}CaF_2$-based mold fluxes was investigated systematically by applying Johnson–Mehl–Avrami (JMA) equation to obtain kinetic parameters. The DSC measurements for $CaO\text{-}SiO_2\text{-}CaF_2$-based mold fluxes with different basicity (mass pct CaO/mass pct SiO_2) were conducted. Based on kinetic parameters obtained, the isothermal melt crystallization mode was determined and compared with that of non-isothermal one.

II. EXPERIMENTAL

A. *Sample Preparation*

The slag samples were prepared using the reagent grade $CaCO_3$, SiO_2, CaF_2, Al_2O_3, MgO, and $NaCO_3$. The reagent powders were mixed well and melted in a platinum crucible with an induction furnace at 1573 K (1300 °C) for 30 min to homogenize chemical composition and then quenched into a cool steel plate. The pre-melted samples were crushed, grounded, sieved by 200 mesh screen, and analyzed by X-ray fluoroscopy. The chemical composition of the pre-melted mold fluxes for the current study is listed in Table I. These pre-melted samples can be utilized to simulate the crystallization behavior of mold slags from commercial casting powders in the continuous casting mold.

B. *DSC Measurement and FE-SEM/EDS Analysis*

The isothermal melt crystallization of $CaO\text{-}SiO_2\text{-}CaF_2$-based mold fluxes was evaluated with DSC (STA 449C; Netzsch Instrument Inc., Germany) measurements in Ar atmosphere at a flow rate of 60 mL/min. As for respective DSC measurement, roughly 50 mg of mold flux powders was subject to heat at a constant heating rate of 20 K (−253 °C)/min from room temperature to 1573 K (1300 °C) in a platinum crucible with diameter of 5 mm. Then the sample was held at 1573 K (1300 °C) for 3 minutes in order to eliminate bubbles and homogenize its chemical composition. Next, the liquid mold flux was cooled at a constant cooling rate of 20 K (−253 °C)/min to different crystallization temperatures T_c determined by the authors' previous study[30] and followed by remaining constant temperature for 120 min. The employed temperature history of DSC measurement is shown in Figure 1. The heat flow released during the crystallization was automatically recorded as a function of time.

The mold flux sample after DSC measurement in a platinum crucible was cut in a longitudinal direction of crucible center position. Then the samples were mounted, polished, and sputtered with a Pt coating of 50 nm for increased electrical conductivity to inhibit charging of the specimen. Finally, the morphology and crystal compositions were examined by field emission scanning electron microscope (FE-SEM; JSM-7401F, JEOL., JAPAN) equipped with energy dispersive X-ray spectroscopy (EDS).

III. RESULTS AND DISCUSSION

A. *Isothermal DSC Measurement*

The isothermal DSC measurements have been carried out considering the non-isothermal melt crystallization behavior[14,30] of mold fluxes B and D. Figure 2 shows the DSC curves of isothermal crystallization for both mold fluxes which melt-crystallized at different crystallization temperatures T_c. As shown in Figure 2, it can be observed that there are two exothermic peaks on DSC curve of mold flux B and D. It should be stressed that the peaks at the beginning of isothermal period in Figure 2 did not originate from the formation of any crystalline phases but arise from the unsteady thermal condition during transition from continuous cooling to isothermal holding. It was confirmed that the crystalline phase corresponding to the exothermic peak on DSC curves represents cuspidine ($3CaO{\cdot}2SiO_2{\cdot}CaF_2$, JCPDS#064710) formation.[30]

As shown in Figure 2, the crystallization exothermic peaks for the cuspidine formation were shifted to longer time and became broader as the crystallization temperature increases, indicating progressively slower crystallization rate. It should be noted from Figure 2(b) that the incubation time for cuspidine formation drastically increases with increasing crystallization temperature. It has been previously reported that undercooling degree for the mold flux D is extremely small,[30] giving rise to the fact that the overall crystallization rate should be governed by the degree of undercooling relevant to free energy change for nucleation.[31–36] Accordingly, the formation of cuspidine phase for mold flux D is more dependent on undercooling degree compared with the case of mold flux B.

Table I. Chemical Composition of the Studied Mold Fluxes in the Present Work

Sample No.	Chemical Composition (Mass Pct)						Basicity
	SiO_2	CaO	MgO	Al_2O_3	Na_2O	F	
B	41.1	38.5	0.8	5	7.3	7	0.94
D	33.4	44.8	0.8	5.4	7.6	7.6	1.34

B. *Isothermal Melt Crystallization Kinetics*

Crystallization of mold fluxes is accompanied by significant heat release, which can be measured by DSC. Based on the fact that the rate of heat release is proportional to the rate of crystallization, the relative degree of crystallinity $X(t)$ can be obtained according to the following equation:

$$X(t) = \frac{\Delta H_t}{\Delta H_{\text{total}}} = \frac{\int_0^t (\mathrm{d}H_c/\mathrm{d}t)\mathrm{d}t}{\int_0^\infty (\mathrm{d}H_c/\mathrm{d}t)\mathrm{d}t}, \quad [1]$$

where ΔH_t is the enthalpy as function of the consuming time from the initial to a given crystallization time and ΔH_{total} is the total enthalpy reached at the end of the isothermal crystallization process. Figure 3 shows the relative degree of crystallinity as function of crystallization time for both mold fluxes B and D at different crystallization temperatures obtained from the crystallization isotherms as exhibited in Figure 2. It can be noted from Figure 3 that sigmoidal curves of mold fluxes B and D for cuspidine formation are shifted toward right along the time axis with increasing the crystallization temperature T_c, indicating that the overall crystallization rate for cuspidine formation decreases with increasing the crystallization temperature.

The isothermal melt crystallization kinetics of mold fluxes can be described by the well-known JMA equation.[37]

$$X(t) = 1 - \exp(-kt^n), \quad [2]$$

where $X(t)$ is the relative degree of crystallinity at a given time t (the incubation time is excluded), n is the Avrami exponent that is associated with the crystallization mode, and k is the effective crystallization rate constant, which is dependent on temperature and rate of nucleation and crystal growth. The values of n and k can be obtained by fitting the double logarithmic form as follows:

$$\log\{-\ln[1 - X(t)]\} = \log k + n \log t \quad [3]$$

The double logarithmic plots of $\log\{-\ln[1-X(t)]\}$ *vs* $\log t$ are shown in Figure 4. From the slope and the intersection of the plots, values of Avrami exponent n and effective crystallization rate constant k can be obtained as summarized in Table II.

Table III shows the values of n and m for various crystallization mode. It is well known that Avrami exponent n is an effective kinetic parameter to determine both the nucleation mode and dimensionality of crystal growth for crystallization.

$$n = n_d + n_n, \quad [4]$$

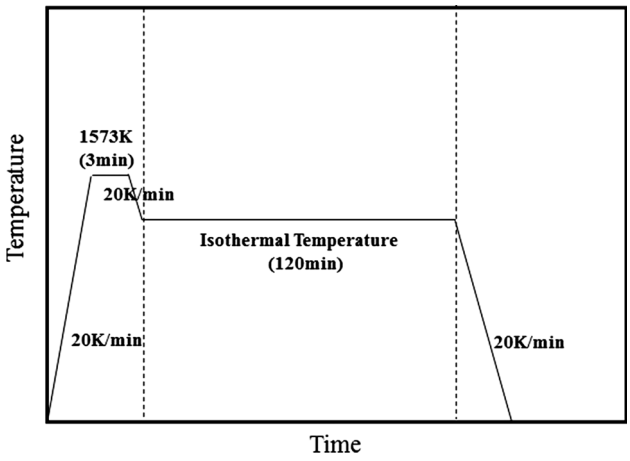

Fig. 1—Thermal profiles in isothermal DSC measurement.

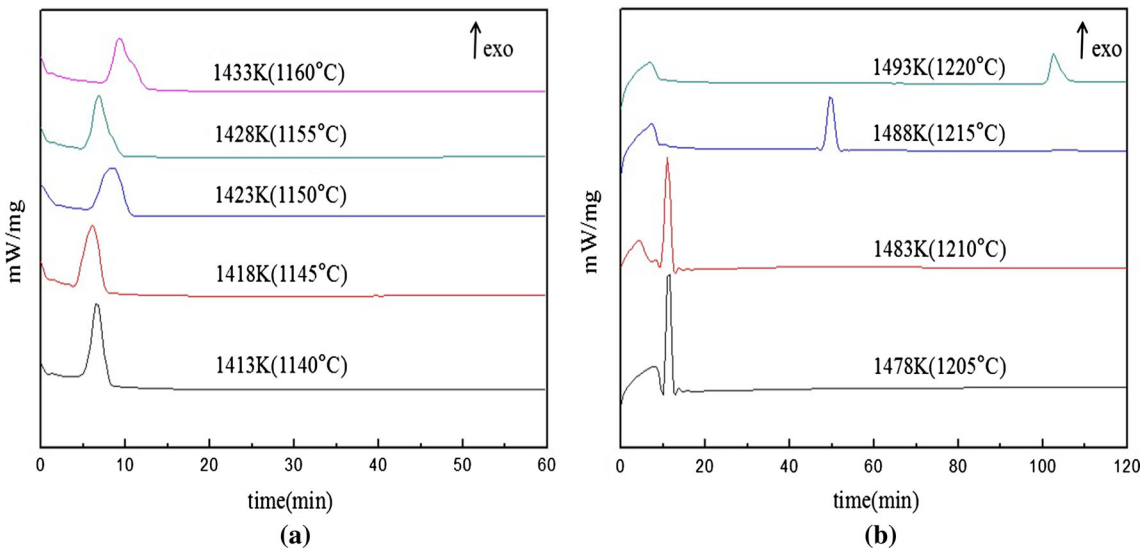

Fig. 2—DSC curves of isothermal crystallization of mold fluxes at the different crystallization temperatures: (*a*) mold flux B, (*b*) mold flux D.

where n_d represents the dimensionality of the crystal growth (*i.e.*, 1, 2, and 3 dimensional) and n_n is the time dependence of the nucleation. It should be noted that n_n can be either 0 or 1, corresponding to instantaneous nucleation and homogeneous nucleation with constant rate, respectively, as can be known in Table III. Considering that the cuspidine crystal growth in mold flux system is 3 dimensional,[14,30] homogeneous nucleation with constant rate corresponds to $n = 4$ and $n_n = 1$, whereas instantaneous nucleation with constant nuclei equals to $n = 3$ and $n_n = 0$. Indeed, nucleation rate could be decreased with time, indicating that n_n corresponds to a number between 0 and 1.[38–40]

It could be observed from Table II that the average values of Avrami exponent n for mold fluxes B and D are 3.1 and 3.4, respectively. After the formation of cuspidine phase, the chemical composition of remaining glassy matrix could be different from that before the cuspidine formation. Consequently, the effective basicity of glassy matrix gets decreased with time, leading to low possibility to form cuspidine phase. In addition, the nucleation could be retarded due to the decrease on available nucleation sites. Since mold flux B with Avrami constant value of 3.1 has a high degree of undercooling,[14] implying that it has large thermodynamic driving force for nucleation, a large number of crystals formation are expected. This will result in the fact that there had been a drastic decrease in available nucleation site and the effective basicity of remaining glassy matrix. Consequently, an instantaneous nucleation occurs initially due to the larger thermodynamic driving forces and followed by a drastic decrease on nucleation rate with time. Therefore, crystallization mode for mold flux B is approximated to instantaneous nucleation with n value of 3, indicating that cuspidine growth is 3 dimensional with instantaneous nucleation controlled. On the other hand, mold flux D has a lower degree of undercooling, indicating that it has smaller thermodynamic driving force for nucleation.[14] Subsequently, the effective basicity of remaining glassy matrix decreases gradually with time, indicating that there had occurred a continuous nucleation with a decrease on nucleation rate. For this reason, the Avrami exponent is in the range between 3 and 4, representing that nucleation rate decreases with time.[38–40] The different nucleation behavior of mold fluxes B and D can be shown schematically in Figure 5, representing that the nucleation rate is the function of time. These results are well in accordance with previous observations by present authors,[14,30] as well as the investigations on crystallization of the mold fluxes using hot thermocouple techniques reported by Li *et al.*,[26] Zhou *et al.*[27] Liu *et al.*,[29] and Kashiwaya *et al.*[41]

It is noted from Table II that the values of the effective crystallization rate constant k for both mold fluxes increase with decreasing the crystallization temperature T_c. Another important kinetic parameter is the crystallization half-time $t_{0.5}$ which is defined as the time at which half-crystallization occurs.

$$t_{0.5} = \left(\frac{\ln 2}{k}\right)^{1/n} \quad [5]$$

It can be known from Figure 6 that the crystallization half-time $t_{0.5}$ of mold fluxes B and D increases with increasing crystallization temperature. This result suggests that the overall crystallization rate should be retarded by the increase in the crystallization temperature, and the crystallization rate will be governed by nucleation rate as suggested by others for melt crystallization.[31–36,42]

The effective crystallization rate constant k can be used to determine the crystallization activation energy through the Arrhenius equation.[42]

$$\frac{1}{n}(\ln k) = \ln k_0 - \frac{E}{RT_c}, \quad [6]$$

where k_0 is a temperature-independent pre-exponential term, n is Avrami exponent, E is effective activation energy, R is the universal gas constant, and T_c is the crystallization temperature. Although both k_0 and E could be considered as being constant over narrow temperature ranges, it could be dependent on temperature over wider ranges. Figure 7 shows the plots of $(1/n)\ln k$ *vs* $1/T_c$ for isothermal crystallization of mold fluxes B and D. The effective activation energy E can be determined from the slope of the plots, and the values of effective activation energy for mold fluxes B and D are determined to be −492 and −882 kJ/mol, respectively, which are similar to activation energies for non-isothermal melt crystallization obtained from Friedman equation.[14] The negative effective activation energies indicate that mold flux melt crystallization should be controlled by the free energy change for nucleation related to the degree of undercooling.[20,43] This result means that the overall crystallization rate for both mold fluxes should be governed by nucleation rate. Based on Turnbull-Fisher theory,[44] nucleation rate can be described as follows:

$$\ln N = \ln N_0 - \frac{E_N}{RT_c} - \frac{\Delta G^*}{RT_c} \quad [7]$$

where N denotes the nucleation rate, N_0 presents a pre-exponential factor, T_c is the crystallization temperature, E_N is activation energy for nucleation, and ΔG^* represents free energy for the formation of a nucleus with critical size. Provided that the value of E_N is considered to be approximately constant, free energy change ΔG^* for the nucleation is inversely proportional to the degree of undercooling.[45]

$$\Delta G^* \approx \frac{1}{(T_m - T_c)^2}, \quad [8]$$

where T_m is the melting temperature of mold flux and $T_m - T_c$ means the degree of undercooling. It is obvious from Eq.[8] that the value of ΔG^* could be extremely large around the melting temperature for molten mold

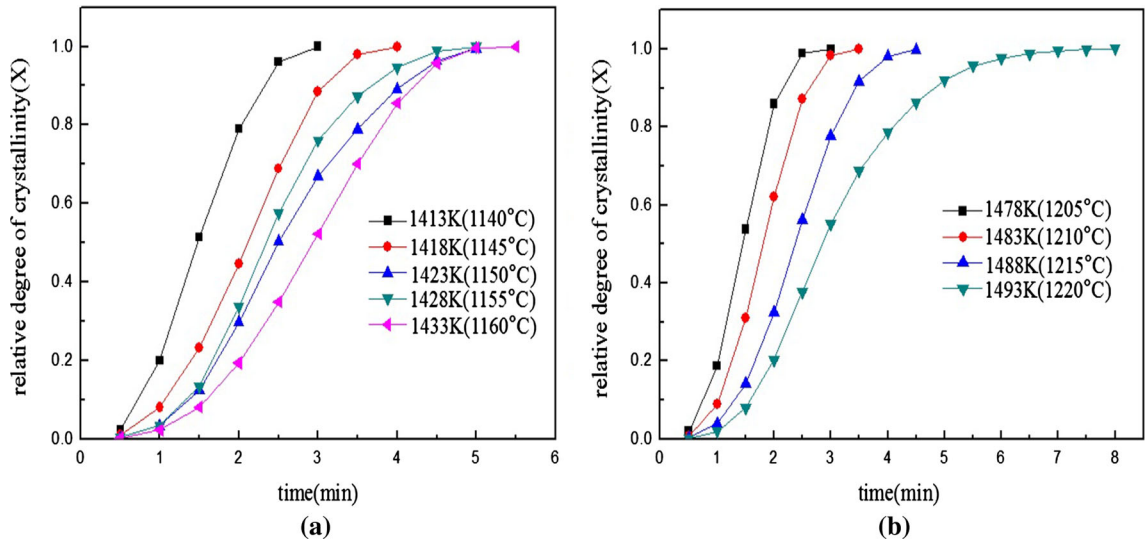

Fig. 3—Relative degree of crystallinity (X) with time for isothermal crystallization at the different crystallization temperatures: (*a*) mold flux B, (*b*) mold flux D.

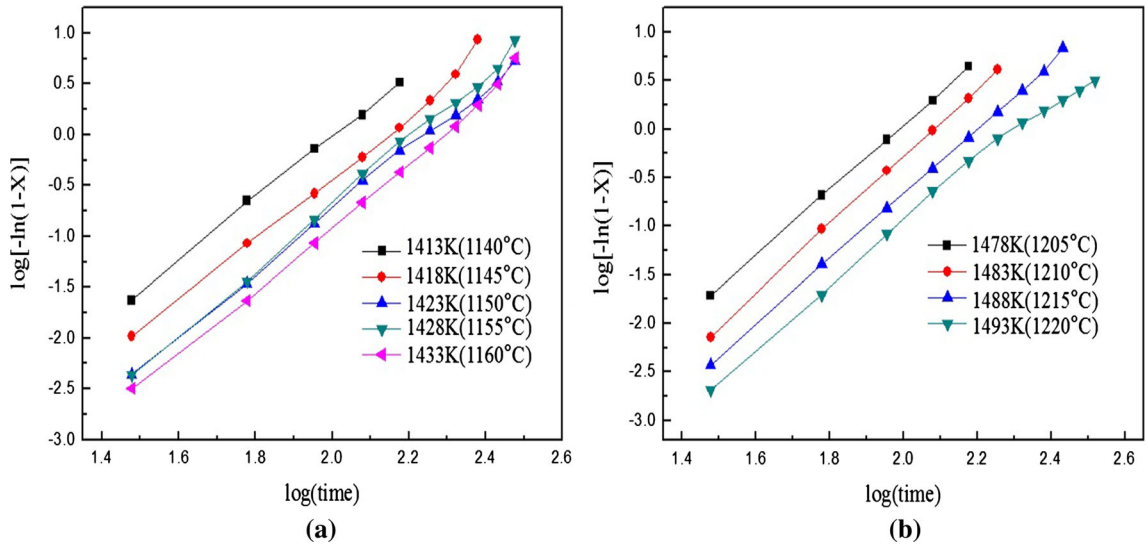

Fig. 4—Plots of $\log[-\ln(1-X)]$ *vs* $\log t$ for isothermal crystallization at the different crystallization temperatures: (*a*) mold flux B, (*b*) mold flux D.

Table II. Results of the Avrami Analysis for Isothermal Crystallization of Mold Fluxes

Sample No.	T_c(K)	n	k	$t_{1/2}$(min)	t_{max}(min)
B	1413	3.03	8.32×10^{-7}	6.59	6.51
	1418	3.11	2.40×10^{-7}	7.48	7.43
	1423	3.10	1.51×10^{-7}	8.02	7.96
	1428	3.22	7.24×10^{-8}	8.16	8.15
	1433	3.19	5.37×10^{-8}	8.73	8.70
D	1478	3.36	2.14×10^{-7}	6.53	6.56
	1483	3.5	5.01×10^{-8}	7.25	7.31
	1488	3.36	4.07×10^{-8}	8.09	8.12
	1493	3.25	3.47×10^{-8}	8.87	8.87

fluxes. This could possibly mean that free energy change for the nucleation becomes extremely small, leading to the fact that the overall crystallization rate should be governed by the nucleation rate. In the interested temperature range, the overall crystallization rate increases with decreasing temperature, indicating that the

Table III. Value of *n* for Different Nucleation and Growth Mode[37,50]

	Crystallization Mode	
	Diffusion Controlled	Interface Reaction Controlled
Constant nucleation rate		
3-Dimensional growth	2.5	4
2-Dimensional growth	2	3
1-Dimensional growth	1.5	2
Instantaneous nucleation		
3-Dimensional growth	1.5	3
2-Dimensional growth	1	2
1-Dimensional growth	0.5	1
Surface nucleation	0.5	1

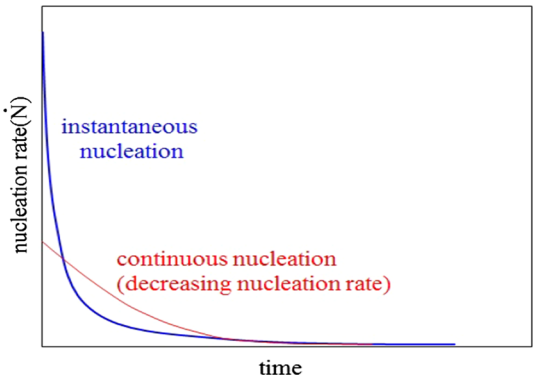

Fig. 5—Schematic diagram of nucleation rate as function of time (blue line for mold flux B, red line for mold flux D).

crystallization shows an anti-Arrhenius behavior with a negative effective activation energy. Similar behavior on the effective activation energy has already been reported for the mold fluxes[14] as well as polymer system.[20,43]

With respect to the degree of undercooling, mold flux B has a larger value than mold flux D; the minimum undercooling has been estimated to be 60.2 K and 9.6 K, respectively.[30] Namely, it could be known from Eqs. [7] and [8] that nucleation rate of mold flux D is relatively smaller than that of mold flux B. Such assertion is strongly supportive that the overall crystallization rate of mold flux D is more dependent on nucleation rate and hence undercooling degree than that of mold flux B, which could be confirmed by the effect of crystallization temperature on the incubation time for both mold fluxes as shown in Figure 2(b).

Given that the nucleation rate in Eq. [7] is only governed by thermodynamic term, the Eq. [7] could be converted to the following Eq. [9] which could be further expressed as following Eq. [10] on basis of Hoffmann theory:[34]

$$\ln N = \ln N_0 - \frac{\Delta G^*}{kT_c} \quad [9]$$

$$\ln N = \ln N_0 - \frac{\chi T_m}{T_c^2 \Delta T}, \quad [10]$$

where T_m is the equilibrium melting point of mold fluxes, χ represents the parameter relevant to heat of fusion and the interfacial energy, and T_c means the crystallization temperature. In general, the overall crystallization rate can be depicted as the reciprocal of $t_{0.5}$. However, in the current study, the overall crystallization rate is quantitatively evaluated by t_{max}, the necessary time for maximum crystallization rate.[34,46] The t_{max} typically takes a form as following Eq. [11]. By combining Eqs. [3], [10], and [11], the following equation [12] can be obtained in order to verify whether the overall crystallization rate is governed solely by the nucleation rate:[34,46]

$$t_{max} = [(n-1)/nk]^{1/n} \quad [11]$$

$$\log t_{max} = C_1 - \frac{C_2}{T_c^2 \Delta T}, \quad [12]$$

where C_1 and C_2 are constants, and ΔT is the undercooling degree. Provided that melt crystallization kinetics of mold fluxes is determined by nucleation rate relevant to the degree of undercooling, it is obvious that the plot of log t_{max} *vs* $1/(T_c^2 \Delta T)$ should be a straight line. The plot of log t_{max} *vs* $1/(T_c^2 \Delta T)$ of mold fluxes B and D is illustrated in Figure 8. As can be seen, the plot for mold flux D shows good linear relationship whereas that for mold flux B shows considerable deviation from linearity. As it is previously mentioned, this is presumably because the overall crystallization rate of mold flux B is relatively more independent from nucleation rate than that of mold flux D.

C. *Crystal Morphology*

Figures 9 and 10 show the FE-SEM back-scattered electron (BSE) images of mold fluxes for cuspidine formation after DSC measurements at various crystallization temperatures. It is observed that the number of cuspidine crystals for mold flux B is larger than those for mold flux D due to nucleation rate relevant to undercooling degree. Moreover, the cuspidine size of mold flux D is larger than that of mold flux B because of the difference in crystallization temperature.

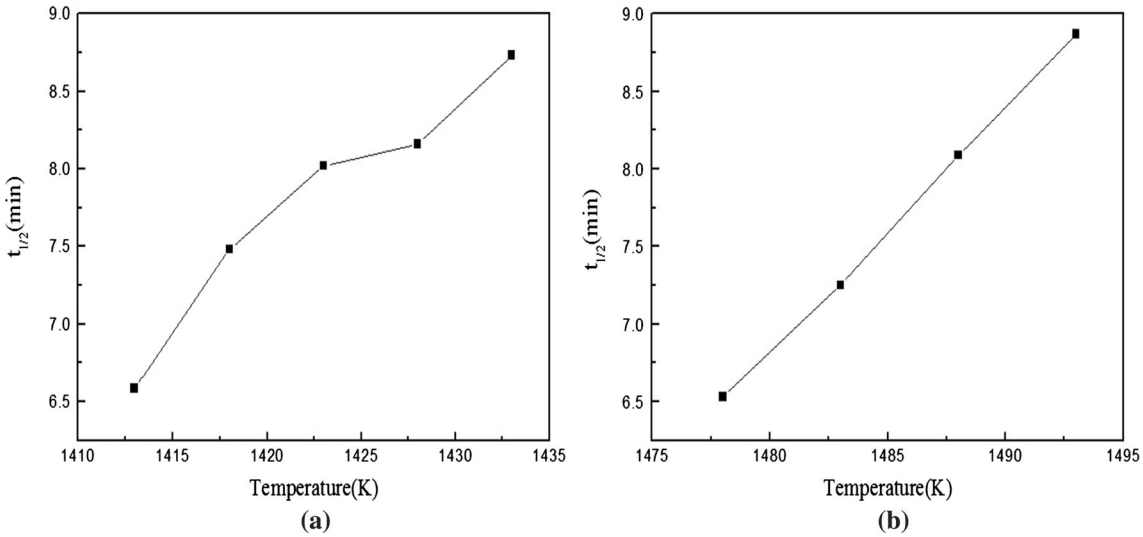

Fig. 6—Plots of half-time of crystallization $t_{1/2}$ *vs* isothermal crystallization temperature: (*a*) mold flux B, (*b*) mold flux D.

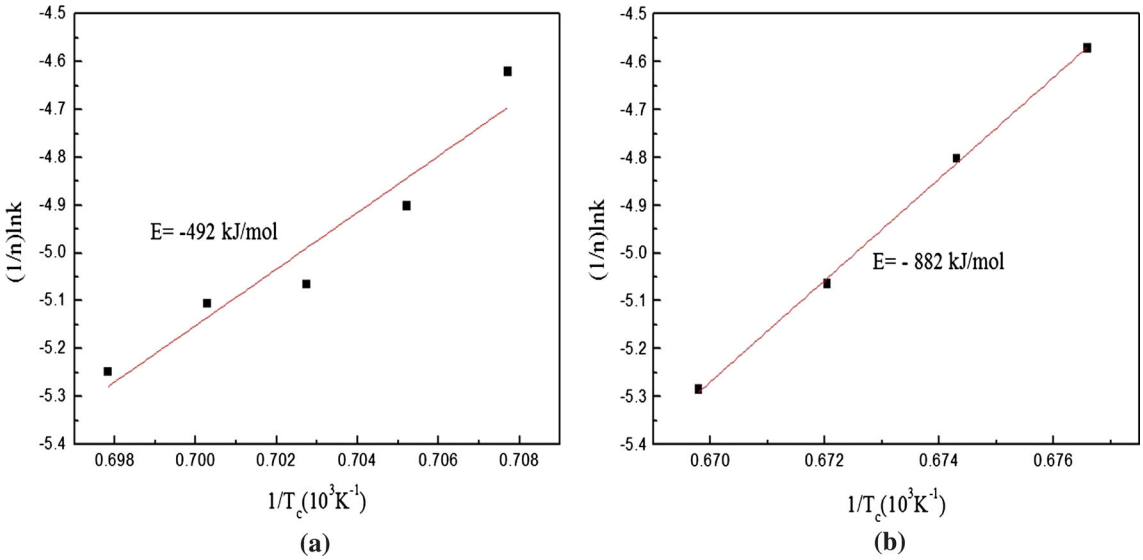

Fig. 7—Plots of $(1/n)$ ln k *vs* $1/T_c$ for isothermal crystallization of mold fluxes: (*a*) mold flux B, (*b*) mold flux D.

It can be seen from Figures 9(a) through (d) that the morphology of cuspidine crystals for mold flux B is mainly dendritic. On the other hand, apart from 1478 K (1205 °C), Figure 10(a), the morphology of cuspidine crystals for mold flux D is recognized as faceted which could be observed in Figures 10(b) through (d). This result is well consistent with Table III explaining the relation between Avrami exponent and morphology of crystal.[27,47]

As it has been previously discussed, the Avrami exponent for cuspidine formation of mold fluxes B and D corresponds to 3.1 and 3.4 respectively. Considering Table III and morphology of cuspidine crystals shown in Figures 9 and 10, the Avrami exponent for cuspidine formation of mold flux B means the 3-dimensional dendritic growth with instantaneous nucleation. This is because the nucleation rate for mold flux B is relatively more rapid than that for mold flux D. On the other hand, Avrami exponent for cuspidine formation of mold flux D corresponds to 3.4. As the Avrami exponent gets closer to 4, it is reported that cuspidine morphology becomes more faceted.[26,48–52] In the current study, Avrami exponent of mold flux D is evaluated as 3.4 which is in between 3 and 4, implying that the cuspidine morphology of mold flux D would have both faceted and dendritic growth. These findings are well in accordance with non-isothermal melt crystallization of mold fluxes B and D.[14]

IV. CONCLUSIONS

The isothermal melt crystallization kinetics of CaO-SiO_2-CaF_2-based mold fluxes with different basicity (CaO/SiO_2) of 0.94 (mold flux B) and 1.34 (mold flux D) was investigated systematically. Based on quantitative

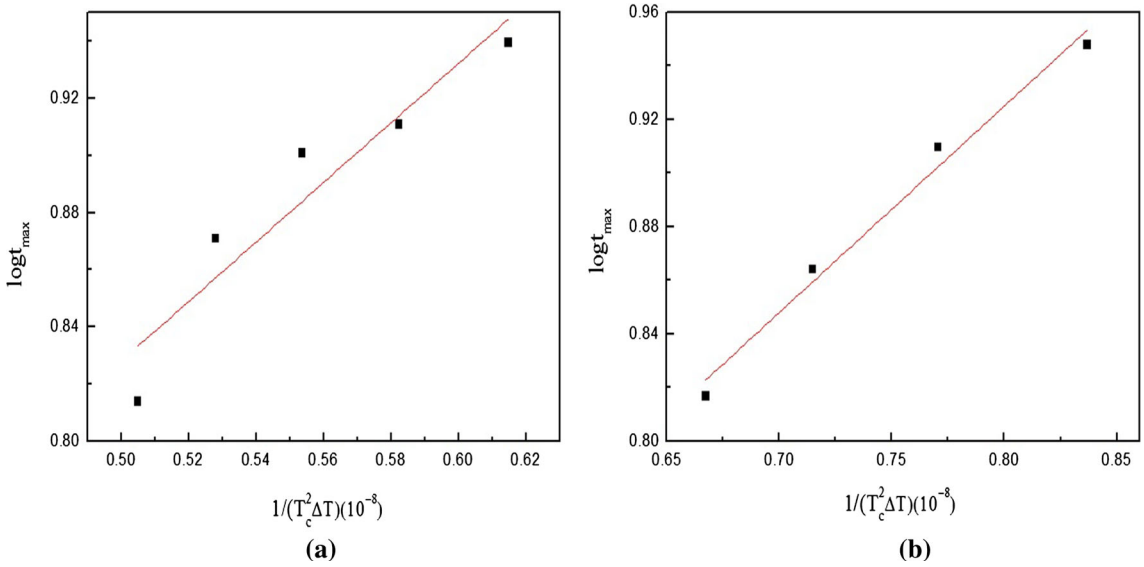

Fig. 8—Plots of log t_{max} *vs* $1/(T_c^2\Delta T)$ for isothermal crystallization of mold fluxes: (*a*) mold flux B, (*b*) mold flux D.

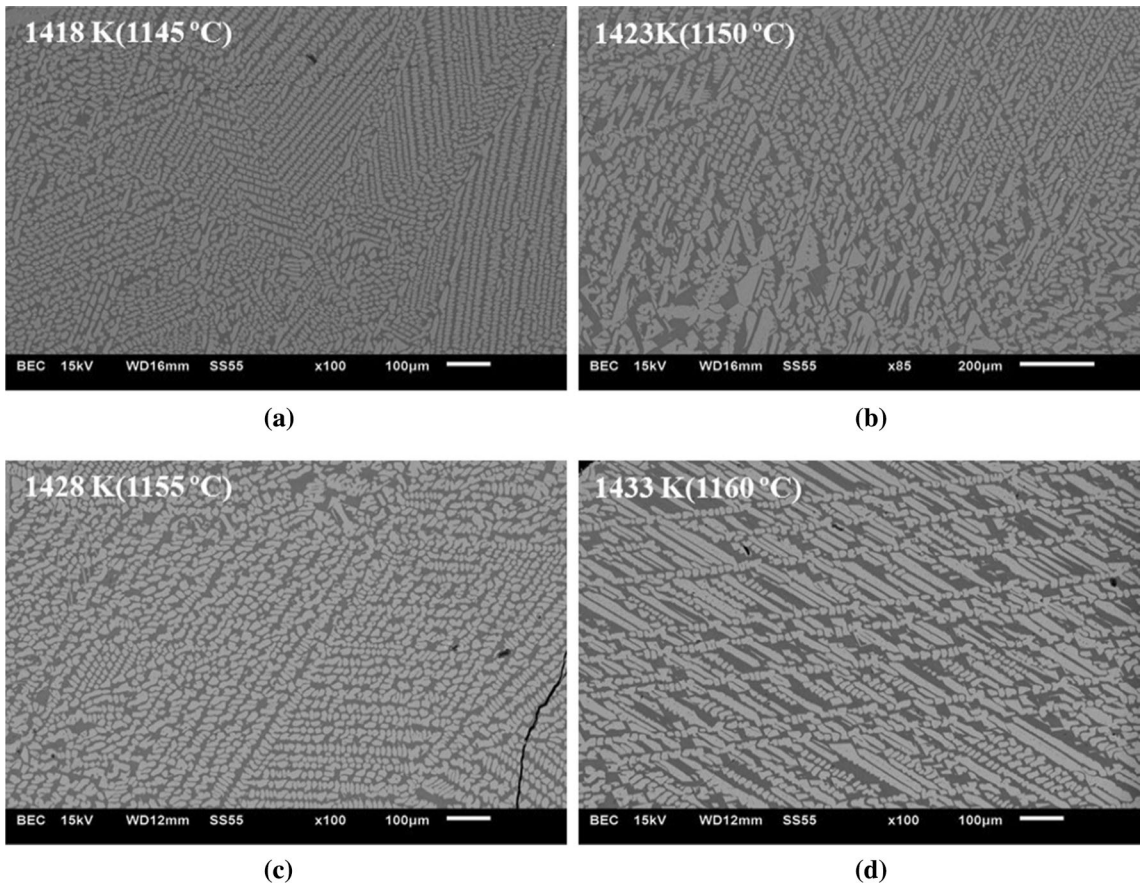

Fig. 9—BSE images of mold flux B after DSC measurement at the different crystallization temperatures: (*a*) 1418 K (1145 °C), (b) 1423 K (1150 °C), (*c*) 1428 K (1155 °C), and (*d*) 1433 K (1160 °C).

kinetic parameters, the crystallization mode was determined, which was compared with the crystal morphology by SEM. The main conclusions were summarized as follows.

1. The average Avrami exponent n of cuspidine formation for mold flux B equals 3.1, indicating that cuspidine growth is 3-dimensional and instantaneous nucleation. On the other hand, the average Avrami

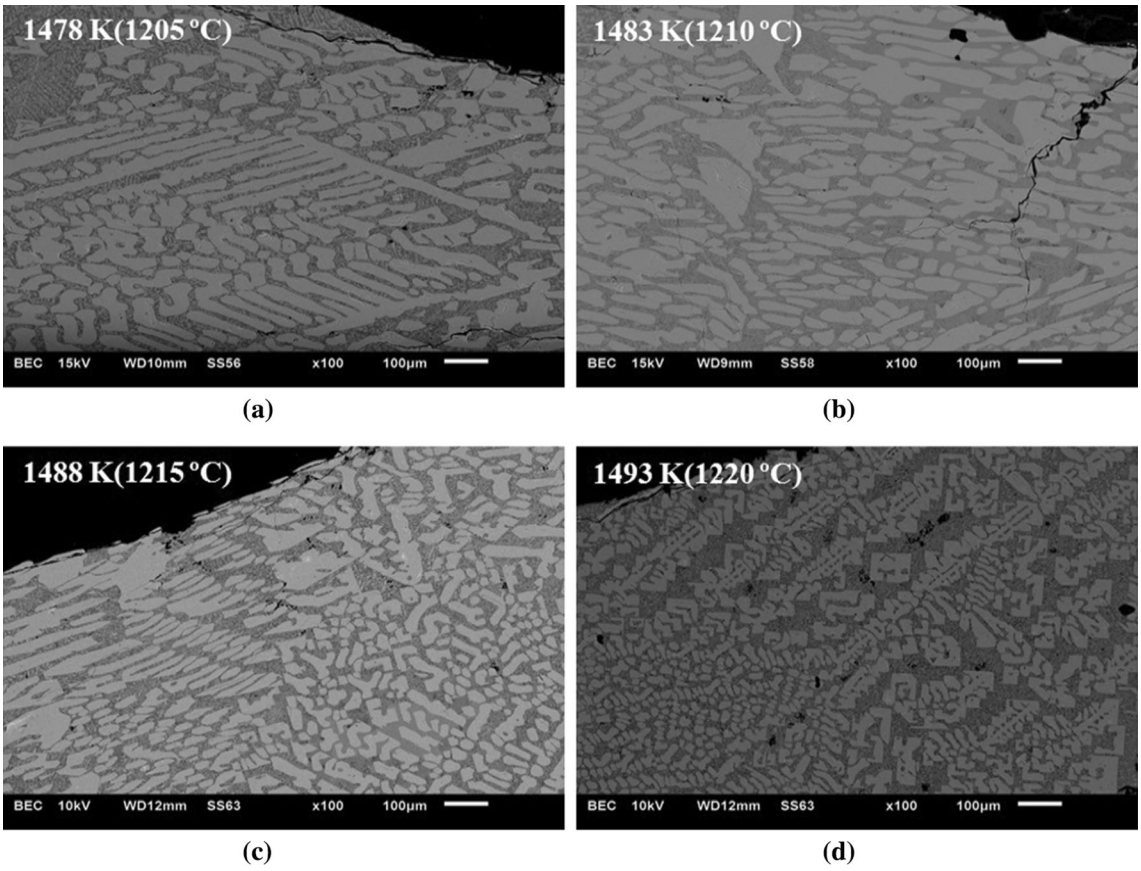

Fig. 10—BSE images of mold flux D after DSC measurement at the different crystallization temperatures: (*a*) 1478 K (1205 °C), (*b*) 1483 K (1210 °C), (*c*) 1488 K (1215 °C), and (*d*) 1493 K (1220 °C).

exponent n of cuspidine formation for mold flux D corresponds to 3.4, meaning that cuspidine growth is 3-dimensional and continuous nucleation.

2. The effective crystallization rate constant k of cuspidine formation for mold fluxes B and D increases with decreasing the crystallization temperature. The crystallization half-time $t_{0.5}$ of cuspidine formation for mold fluxes B and D increases with increasing the crystallization temperature. These results suggest that the overall crystallization rate was retarded by the increase in temperature, which implies that the crystallization is controlled by nucleation over crystallization temperature range.
3. The effective activation energy of cuspidine formation for mold fluxes B and D is determined to be −492 and −882 kJ/mol, respectively. The negative values of effective activation energy of cuspidine formation for mold fluxes B and D mean the anti-Arrhenius behaviors, giving rise to the fact that mold fluxes crystallization for the cuspidine formation is determined by thermodynamic term of nucleation which is related to undercooling degree.
4. The morphology of cuspidine crystals for mold flux B is mainly dendritic at larger undercooling, whereas the morphology of cuspidine crystals for mold flux D is mainly faceted. The number of cuspidine crystals for mold flux B is larger than that for mold flux D. These results well supported the isothermal crystallization kinetics.

REFERENCES

1. K.C. Mills, A.B. Fox, Z. Li, and R.P. Thackray: *Ironmak. Steelmak.*, 2005, vol. 32, pp. 26–34.
2. J.W. Cho, H. Shibata, T. Emi, and M. Suzuki: *ISIJ Int.*, 1998, vol. 38, pp. 268–75.
3. J.W. Cho, H. Shibata, T. Emi, and M. Suzuki: *ISIJ Int.*, 1998, vol. 38, pp. 440–46.
4. J.W. Cho, T. Emi, H. Shibata, and M. Suzuki: *ISIJ Int.*, 1998, vol. 38, pp. 834–42.
5. M. Hayashi, R.A. Abas, and S. Seetharaman: *ISIJ Int.*, 2004, vol. 44, pp. 691–97.
6. Y. Kobayashi, R. Maehashi, R. Endo, and M. Susa: *ISIJ Int.*, 2013, vol. 53, pp. 1725–31.
7. S. Ozawa, M. Susa, T. Goto, R. Endo, and K.C. Mills: *ISIJ Int.*, 2006, vol. 46, pp. 413–19.
8. M. Dapiaggi, G. Artioli, C. Righi, and R. Carli: *J. Non-Cryst. Solids*, 2007, vol. 353, pp. 2852–60.
9. T. Watanabe, H. Hashimoto, M. Hayashi, and K. Nagata: *ISIJ Int.*, 2008, vol. 48, pp. 925–33.
10. Z. Wang, Q. Shu, and K. Chou: *Metall. Mater. Trans. B*, 2013, vol. 44B, pp. 606–13.
11. S.Y. Choi, D.H. Lee, D.W. Shin, S.Y. Choi, J.W. Cho, and J.M. Park: *J. Non-Cryst. Solids*, 2004, vol. 345&346, pp. 157–60.
12. L. Gan, C. Zhang, J. Zhou, and F. Shangguan: *J. Non-Cryst. Solids*, 2012, vol. 358, pp. 20–24.
13. C.B. Shi, M.D. Seo, H. Wang, J.W. Cho, and S.H. Kim: *Metall. Mater. Trans. B*, 2015, vol. 46B, pp. 345–56.

14. M.D. Seo, C.B. Shi, H. Wang, J.W. Cho, and S.H. Kim: *J. Non-Cryst. Solids*, 2015, vol. 412, pp. 58–65.
15. M. Joshi and B.S. Butola: *Polymer*, 2004, vol. 45, pp. 4953–68.
16. S.P. Lonkar, S. Morlat-Therias, N. Caperaa, F. Leroux, J.L. Gardette, and R.P. Singh: *Polymer*, 2009, vol. 50, pp. 1505–15.
17. T. Bin, J. Qu, L. Liu, Y. Feng, S. Hu, and X. Yin: *Thermochim. Acta*, 2011, vol. 525, pp. 141–49.
18. T. Liu, Z. Mo, S. Wang, and H. Zhang: *Polym. Eng. Sci.*, 1997, vol. 37, pp. 568–75.
19. S. Vyazovkin: *Macromol. Rapid Commun.*, 2002, vol. 23, pp. 771–75.
20. S. Vyazovkin and N. Sbirrazzuol: *J. Phys. Chem.*, 2003, vol. 107, pp. 882–88.
21. C.B. Shi, H. Wang, M.D. Seo, J.W. Cho, and S.H. Kim: *Metall. Mater. Trans. B*, 2014, vol. 45B, pp. 1987–91.
22. H.L. Friedman: *J. Polym. Sci. C*, 1964, vol. 6, pp. 183–95.
23. G.Z. Papageorgioua, D.S. Achiliasa, S. Nanakia, T. Beslikasb, and D. Bikiaris: *Thermochim. Acta*, 2010, vol. 511, pp. 129–39.
24. H. Liang, F. Xie, F. Guo, B. Chen, F. Luo, and Z. Jin: *Polym. Bull.*, 2008, vol. 60, pp. 115–27.
25. N. Apiwanthanakorn, P. Supaphol, and M. Nithitanakul: *Polym. Test.*, 2004, vol. 23, pp. 817–26.
26. J. Li, W. Wang, J. Wei, D. Hyang, and H. Matsuura: *ISIJ Int.*, 2012, vol. 52, pp. 2220–25.
27. L. Zhou, W. Wang, F. Ma, J. Li, J. Wei, H. Matsuura, and F. Tsukihashi: *Metall. Mater. Trans. B*, 2014, vol. 43B, pp. 354–62.
28. J. Li, X. Wang, and Z. Zhang: *ISIJ Int.*, 2011, vol. 51, pp. 1396–402.
29. H. Liu, G. Wen, and P. Tang: *ISIJ Int.*, 2009, vol. 6, pp. 843–50.
30. M.D. Seo, C.B. Shi, J.W. Cho, and S.H. Kim: *Metall. Mater. Trans. B*, 2014, vol. 45B, pp. 1874–86.
31. C. Jiao, Z. Wang, X. Liang, and Y. Hu: *Polym. Test*, 2005, vol. 24, pp. 71–80.
32. P. Supaphol: *J. Appl. Polym. Sci.*, 2000, vol. 78, pp. 338–54.
33. P. Supaphol and J.E. Spruiell: *J. Appl. Polym. Sci.*, 2000, vol. 75, pp. 44–59.
34. M. Liu, Q. Zhao, Y. Wang, C. Zhang, Z. Mo, and S. Cao: *Polymer*, 2003, vol. 44, pp. 2537–45.
35. X.F. Lu and J.N. Hay: *Polymer*, 2001, vol. 42, pp. 9423–31.
36. B.J. Chisholm and J.G. Zimmer: *J. Appl. Polym. Sci.*, 2000, vol. 76, pp. 1296–307.
37. M. Avrami: *J. Chem. Phys.*, 1939, vol. 7, pp. 1103–12.
38. M.M. Krzmanc, U. Dosler, and D. Suvorov: *J. Eur. Ceram. Soc.*, 2011, vol. 31, pp. 2211–19.
39. E.D. Dill, J.C.W. Folmer, and J.D. Martin: *J. Am. Chem. Soc.*, 2013, vol. 25, pp. 3941–51.
40. E.D. Zanotto and A. Galhardi: *J. Non-Cryst. Solids*, 1988, vol. 104, pp. 73–80.
41. Y. Kashiwaya, C.E. Cicutti, and A.W. Cramb: *ISIJ Int.*, 1998, vol. 38, pp. 357–65.
42. P. Cebe and S.D. Hong: *Polymer*, 1986, vol. 27, pp. 1183–92.
43. G.Z. Papageorgiou, D.S. Achilias, D.N. Bikiaris, and G.P. Karayannidis: *Thermochim. Acta*, 2005, vol. 427, pp. 117–128.
44. D. Turnbull and J.C. Fisher: *Chem. Phys.*, 1949, vol. 17, p. 71.
45. J.M. Schultz: *Polymer Material Science*, Prentice Hall, Englewood, 1974.
46. C.C. Lin: *Polym. Eng. Sci.*, 1983, vol. 23, pp. 113–16.
47. D.R. MacFarlane and M. Fragoulis: *Phys. Chem. Glasses*, 1986, vol. 37 (6), pp. 228–34.
48. S.S. Jung and I. Sohn: *Metall. Mater. Trans. B*, 2012, vol. 43B, pp. 1530–39.
49. C. Orrling, S. Sridhar, and A.W. Cramb: *ISIJ Int.*, 2000, vol. 40, pp. 877–85.
50. R.J. Kirkpatrick: *Am. Mineral.*, 1975, vol. 60, pp. 798–814.
51. J. Huelens, B. Blanpain, and N. Moelans: *J. Eur. Ceram. Soc.*, 2011, vol. 31, pp. 1873–79.
52. D. Li and D.M. Herlach: *Phys. Review. Lett.*, 1996, vol. 77.